

## **Rapid Transpacific Transport in Autumn Observed by the A-train Satellites**

Can Li<sup>1,2</sup>, N. Christina Hsu<sup>2</sup>, Nickolay A. Krotkov<sup>2</sup>, Qing Liang<sup>3,2</sup>, Kai Yang<sup>4,2</sup> and Si-Chee Tsay<sup>2</sup>

<sup>1</sup>Earth System Science Interdisciplinary Center, University of Maryland, College Park, MD, USA.

<sup>2</sup>Goddard Space Flight Center, National Aeronautics and Space Administration, Greenbelt, MD, USA.

<sup>3</sup>Universities Space Research Association, Columbia, MD, USA

<sup>4</sup>Department of Atmospheric and Oceanic Science, University of Maryland, College Park, MD, USA.

Revised for Submission to

*Journal of Geophysical Research – Atmospheres*

2011JD016626

October 30, 2011

## **Abstract**

Transpacific transport of dust and pollutants is well documented for spring, but less so for other seasons. Here we investigate rapid transpacific transport in autumn utilizing the A-train satellites. In three episodes studied as examples, SO<sub>2</sub> plumes over East Asia were detected by the Ozone Monitoring Instrument aboard the Aura satellite, and found to reach North America in 5-6 days. They were likely derived from anthropogenic sources, given that identical transport patterns of CO, a tracer for incomplete combustion, were simultaneously observed by the Aqua satellite. Trajectory analysis and meteorological data were employed to explore the meteorological circumstances surrounding these events: like many of their counterparts in spring, all three plumes were lifted to the free troposphere in warm conveyor belt associated with mid-latitude wave cyclones, and their migration to downwind region was regulated by the meteorology over the East Pacific. These cases provide further evidence that a fraction of SO<sub>2</sub> could escape wet scavenging, and be transported at much greater efficiency than NO<sub>x</sub> (NO + NO<sub>2</sub>). An analysis of the SO<sub>2</sub> and CO data from September to November during 2005-2008 found 16 SO<sub>2</sub> long-range transport episodes, out of 62 Asian outflow events. While the counts are sensitive to the choice of criteria, they suggest that the long-range transport of Asian sulfur species occurs quite frequently, and could exert strong impacts on large downstream areas. This study also highlights the importance of transpacific transport in autumn, which has thus far been rarely studied and deserves more attention from the community.

**Key Words:** long-range transport, SO<sub>2</sub>, CO, East Asia, A-train satellites.

## 1. Introduction

There is mounting evidence that Asian pollutants can travel far away from their source regions, in some cases across the Pacific [e.g., *Barletta et al.*, 2009; *Jaffe et al.*, 1999, 2003; *Walker et al.*, 2010]. Because of their potential large-scale impacts [e.g., *Berntsen et al.*, 1999; *Brown-Steiner and Hess*, 2011; *Cooper et al.*, 2010; *Fiore et al.*, 2009; *Heald et al.*, 2006; *Jacob et al.*, 1999; *Zhang et al.*, 2008], such transpacific transport events have been the primary focus of several recent field campaigns [e.g., *Jacob et al.*, 2003; *Parrish et al.*, 2004; *Singh et al.*, 2009]. These experiments provide valuable insights into the meteorological mechanisms for transpacific transport, particularly for relatively long-lived pollutants such as CO. It is now recognized that mid-latitude wave cyclones play a crucial part in exporting Asian pollution [e.g., *Liu et al.*, 2003; *Yienger et al.*, 2000], particularly in the cold season [*Liang et al.*, 2004], through advection in the boundary layer behind cold fronts [e.g., *Carmichael et al.*, 2003; *Kaneyasu et al.*, 2000] and lifting in the warm conveyor belt (WCB) [e.g., *Bey et al.*, 2001; *Cooper et al.*, 2004]. Convective transport is more significant in summer [e.g., *Liang et al.*, 2007], but can also be sizable in spring [*Dickerson et al.*, 2007]. Once displaced from their source region, the destination of pollutants is largely determined by the highly variable meteorological setup in the downstream area [e.g., *Fisher et al.*, 2010; *Liang et al.*, 2005], which is responsible for the episodic nature of transpacific transport and its strong interannual variability [e.g., *Liang et al.*, 2005; *Pfister et al.*, 2010]. It is worth mentioning that most of the existing studies focus on spring [*Wuebbles et al.*, 2007], and few deal with autumn, a season also featuring frequent cyclonic activity and potentially strong long-range transport.

Compared to long-lived air pollutants, the long-range transport of short-lived pollutants is not as well documented. For Asian NO<sub>x</sub> or SO<sub>2</sub> (lifetime in the boundary layer: hours to days) to cross the Pacific, they need to be first lifted into the free troposphere (FT) by WCB or convection, where stronger winds and extended chemical lifetime greatly enhance their potential for long-range transport [Holzer *et al.*, 2003]. The export efficiency of short-lived species is however typically low, as substantial rainfall and washout normally occur during their ascent [Eckhardt *et al.*, 2004]. Only 10-20% of East Asian NO<sub>y</sub> (reactive nitrogen, NO + NO<sub>2</sub>+NO<sub>3</sub> + 2(N<sub>2</sub>O<sub>5</sub>) + HNO<sub>3</sub> + HONO + HNO<sub>4</sub> + peroxyacyl nitrates + organic nitrate) can reach the FT [Koike *et al.*, 2003; Miyazaki *et al.*, 2003], as corroborated by the small NO<sub>y</sub>/CO ratio observed in transpacific plumes [Nowak *et al.*, 2004].

The overall export efficiency for Asian SO<sub>x</sub> (SO<sub>2</sub> + sulfate) into the FT is similarly low [15-20%, Koike *et al.*, 2003], but sizable (up to ~1 ppb) anthropogenic SO<sub>2</sub> has been observed thousands of kilometers away from Asia [Brock *et al.*, 2004; Dunlea *et al.*, 2009; Tu *et al.*, 2004]. It has been proposed that a larger fraction of SO<sub>x</sub> could remain as SO<sub>2</sub> prior to the frontal lifting, due to its relatively slow gas-phase oxidation (in comparison to the formation of nitrate and some secondary organic aerosols). Part of this remaining SO<sub>2</sub>, a moderately soluble gas, can survive wet scavenging during the ascent in WCB [Brock *et al.*, 2004]. While sulfate formed prior to the frontal lifting is often washed out, new sulfate production from the SO<sub>2</sub> that has survived the process is expected during the transport. Indeed, sulfate is often the dominant species in fine particles sampled in transpacific plumes [e.g., Leaitch *et al.*, 2009; Dunlea *et al.*, 2009] and the long-range transport of Asian SO<sub>x</sub> could exert non-negligible impacts on the

aerosol loading, air quality, and visibility over large downstream areas [*Heald et al.*, 2006; *Park et al.*, 2004; *van Donkelaar et al.*, 2008]. However, it remains unclear how often  $\text{SO}_x$  transpacific events occur, and how much Asian  $\text{SO}_x$  is transported to North America. To gain a better understanding of these important issues, long-term, large-scale observations are needed to complement more detailed, short-term field measurements and model simulations.

Here we explore the long-range transport of Asian pollutants utilizing data from the Aqua, Aura, and CALIPSO satellites. Flying in close formation, they are part of the polar-orbiting afternoon (1:30 pm local solar time) A-train constellation, and provide highly complementary global measurements which have been instrumental in previous studies on long-range transport [e.g., *Heald et al.*, 2006; *Yu et al.*, 2008; *Zhang et al.*, 2008]. While satellite retrievals are still too uncertain to directly quantify the transport of  $\text{SO}_x$ , they can help identify long-range transport events and estimate their frequency over an extended period of time. In this study, we analyze satellite retrievals of  $\text{SO}_2$ , a short-lived species, and CO, a relatively long-lived tracer for incomplete combustion, to distinguish rapid long-range transport of anthropogenic pollution. We also focus on autumn, presenting evidence that transpacific transport in this transition season could be important.

## **2. Data and Method**

### 2.1 Satellite data

#### 2.1.1 OMI $\text{SO}_2$ data

Launched in 2004 onboard the NASA Aura satellite [*Schoeberl et al.*, 2006], the Dutch-Finnish Ozone Monitoring Instrument (OMI) is a hyperspectral UV spectrometer

featuring both daily global coverage and fine spatial resolution ( $13 \times 24 \text{ km}^2$  at nadir) [Levelt *et al.*, 2006]. Two operational algorithms are currently in use for retrieving  $\text{SO}_2$  column density from the OMI data: the Band Residual Difference (BRD) algorithm [Krotkov *et al.*, 2006; 2008] designed for maximizing sensitivity to boundary layer pollution [e.g., Li *et al.*, 2010a], and the Linear Fit (LF) algorithm [Yang *et al.*, 2007] primarily for retrieving plumes with high  $\text{SO}_2$  loading (e.g., those from volcanic eruptions). As the long-range transport of  $\text{SO}_2$  likely occurs in the FT and BRD retrievals over the North Pacific storm track can be severely restricted by cloudy scenes, in this study we used the collection 3 level 2 LF middle troposphere (TRM)  $\text{SO}_2$  column amount, available for pixels with cloud height below  $\sim 7 \text{ km}$ .

In the LF algorithm an initial estimate of the total ozone and effective cloud fraction (CF) is first derived using the TOMS total ozone algorithm [Bhartia and Wellemeyer, 2002] and assuming no  $\text{SO}_2$ . The radiance residuals at 10 wavelengths between 308.7 and 375 nm are then calculated with a vector forward model radiative transfer code, for which cloudy scenes are treated as a mixture of two opaque Lambertian surfaces, one at the terrain pressure and the other at OMI-retrieved Optical Centroid Radiative Cloud Pressure [Joiner and Vasilkov, 2006]. If  $\text{SO}_2$  is present, the resulting radiance residuals contain spectral structures correlated with the  $\text{SO}_2$  absorption cross section, as well as contributions from other yet undetermined error sources. Interference from the latter is reduced with a sliding median residual correction method [Yang *et al.*, 2007]. The algorithm then simultaneously adjusts total  $\text{SO}_2$ , ozone, and a quadratic parameterization of CF to minimize the radiance residuals for different subsets of the 10 wavelengths. To obtain the subsets, the shorter wavelength bands (up to 322 nm) are

removed one at a time, and the largest SO<sub>2</sub> amount from these subsets is the final estimate. An important *a priori* assumption in the retrieval is the height of the SO<sub>2</sub> plume or the center of mass altitude (CMA). The TRM SO<sub>2</sub> corresponds to a CMA of ~7 km, making it suitable for studying transport in the mid-/upper troposphere.

The 1- $\sigma$  noise of TRM retrievals over presumably clean background tropical and mid-latitude areas is estimated at 0.3 DU (Dobson Unit, 1 DU =  $2.69 \times 10^{16}$  molecules/cm<sup>2</sup>). Biases due to latitude and viewing angle are ~0.1 DU but increase with solar zenith angle (SZA). We used retrievals with SZA < 70° in this study and rejected pixels affected by the OMI row anomaly (abnormal L1B radiance signals for specific rows on the CCD detector affecting particular viewing directions near nadir and western part of the OMI swath, see <http://www.knmi.nl/omi/research/product/rowanomaly-background.php> ), before gridding the data to 0.5° × 0.5° resolution. SO<sub>2</sub> resided at altitudes < 7 km is underestimated in the TRM data, an artifact that can be corrected for if the actual SO<sub>2</sub> vertical distribution is known. In the absence of this knowledge, OMI SO<sub>2</sub> data were used qualitatively here as a tracer for short-lived anthropogenic pollutants. An example for the quantitative application of the OMI SO<sub>2</sub> data is given in our previous work [Li *et al.*, 2010b].

#### 2.1.2 AIRS CO data and CALIPSO vertical feature mask

The Atmospheric Infrared Souder aboard NASA's Aqua satellite has 2378 channels over a wide spectral range from 600 to 2655 cm<sup>-1</sup> (15.38 to 3.75  $\mu$ m), and covers about 70% of the Earth each day [Aumann *et al.*, 2003]. In the AIRS version 5 (V5) algorithm, 36 channels in the spectral range of 2181.49 -2221.12 cm<sup>-1</sup> are used to retrieve CO on nine trapezoidal pressure levels sampled from the 100 AIRS standard

layers [McMillan *et al.*, 2011]. Limited by the spectral resolution in the CO region, the AIRS CO retrieval averaging kernels (reflect retrieval sensitivity to CO variations at different altitudes) have broad peaks in the middle troposphere (~500 hPa). The sum of the elements along the main diagonal of the averaging kernel matrix, or the degrees of freedom (DOF), represents the information content for the retrieval: a value over 0.5 indicates that > 50% of a particular retrieval is determined from the AIRS radiances, other than the first-guess profile. The DOF of AIRS CO retrievals is typically ~0.8 and rarely exceeds 1.5 [McMillan *et al.*, 2011]. AIRS CO retrievals are available over partially cloudy scenes, although a weak anti-correlation exists between DOF and cloudiness, reflecting the reduction in CO information due to increasing cloud cover [McMillan *et al.*, 2011]. In this study, the total CO column from AIRS is used as a tracer for relatively long-lived anthropogenic pollutants. Following Fisher *et al.* [2010], we only included daytime retrievals with DOF > 0.5 and surface temperature > 250 K. Level 2 data were binned to  $1^\circ \times 1^\circ$  grid cells. Yurganov *et al.* [2010] compared AIRS total column CO to ground-based retrievals, noticing that for northern hemisphere the bias was generally within  $\pm 10\%$  and even smaller between June and November.

The primary instrument aboard the CALIPSO (Cloud-Aerosol Lidar and Infrared Pathfinder Satellite Observations) satellite is the CALIOP (Cloud-Aerosol Lidar with Orthogonal Polarization), a two-wavelength polarization lidar [Winker *et al.*, 2009]. Here version 3.01 (V3) level 2 vertical feature mask (VFM) product was employed to determine the plume height during transport. VFM contains information about the location (latitude, longitude, and altitude) and type of various detected features such as aerosols and clouds. While the feature location is fairly accurate, the retrieved feature

type is subject to larger uncertainties [Liu *et al.*, 2009]. For example, dense dust layers can be misclassified as clouds [e.g., Di Pierro *et al.*, 2011], an artifact partially alleviated in the V3 product by introducing additional diagnostic parameters for cloud-aerosol discrimination. The nighttime CALIPSO data have greater signal-to-noise ratio, but in this study we used daytime VFM data coincident with OMI and AIRS measurements. Some improvements achieved in the V3 daytime calibration were highlighted in a recent validation study [Rogers *et al.*, 2011].

## 2.2 Model and meteorological data

For trajectory calculation, we employed the NOAA Air Resource Laboratory HYSPLIT (HYbrid Single-Particle Lagrangian Integrated Trajectory) model [Draxler and Rolph, 2003], along with the NCEP Global Data Assimilation System (GDAS) meteorological fields having  $1^\circ \times 1^\circ$  horizontal resolution and 23 vertical levels. 120-hr forward trajectories from 12 different starting heights (1.5, 2.0, 2.5, 3.0, 3.5, 4.0, 4.5, 5.0, 5.5, 6.0, 7.0, and 8.0 km above ground level, AGL) were initiated from  $0.5^\circ \times 0.5^\circ$  grid cells covering the initial domain of SO<sub>2</sub> plumes. Each trajectory was tagged with TRM SO<sub>2</sub> for the corresponding cell. The trajectory tracer SO<sub>2</sub> for different starting heights was re-sampled based on satellite overpass time (to the nearest hour) and orbit, and compared to OMI measurements for a rough estimate of the initial plume height. It should be pointed out that Asian outflow often has complicated, multi-layer vertical structure, and our inferred plume height should be viewed as an approximation of the actual transport altitude. On the other hand, the TRM algorithm is insensitive to the boundary layer outflow and the plume height estimated this way essentially represents the part of the plume possessing the greatest potential for long-range transport. For the same

reason, the SO<sub>2</sub> plumes are generally elevated and about 1-2 days displaced from their sources when first identified in the TRM data. 36-48 hour (hr) backward trajectories were used to determine their source regions.

In addition to the trajectories, the NASA Modern Era Retrospective-Analysis for Research and Applications [MERRA, *Rienecker et al.*, 2011] meteorological data provide information about the meteorological conditions surrounding the transpacific events. The MERRA assimilated data are generated using the GEOS-5 atmospheric data assimilation system with a grid of 1/3° longitude × 0.5° latitude × 72 layers. The data set used here has been averaged to 1.25° × 1.25° and 42 vertical layers.

### **3. SO<sub>2</sub> long-range transport in autumn: examples and meteorological mechanism**

We started by visually inspecting daily OMI TRM SO<sub>2</sub> maps during autumn (September, October, and November) 2005-2010, excluding periods influenced by large volcanic eruptions (Aura Cloud/Aerosol/SO<sub>2</sub> working group, personal communication, 2010). A number of regional SO<sub>2</sub> outflow plumes covering thousands of km<sup>2</sup> were found over Northeast Asia, and some appeared to travel far downwind. Because of the uncertainties in the current operational SO<sub>2</sub> retrievals, we employed AIRS CO data and trajectory modeling to validate OMI-observed outflow and transport events. The methodology is demonstrated in this section using three prominent, well-defined SO<sub>2</sub> transport cases. Their transpacific transit time, meteorological circumstances, and the SO<sub>2</sub> transport efficiency are also discussed.

#### **3.1 Case 1: 8 October 2006**

We first discuss a transpacific case occurred in October 2006. On 8 October, large SO<sub>2</sub> loading was observed by OMI over northeastern China (Figure 1a). Over the

next few days, this plume first moved northeastward, reaching the north tip of the Sakhalin Island on the 9<sup>th</sup> (Figure 1b), and the Kamchatka Peninsula on the 10<sup>th</sup> (Figure 1c), before veering to the east. The front edge of the SO<sub>2</sub> plume passed just south of the Aleutian Islands on the 11<sup>th</sup> (Figure 1d) and arrived in the Gulf of Alaska and North America about one day later (Figure 1e). An overview of the movement of the SO<sub>2</sub> plume is also given in Figure 2a. AIRS data (Figures 1j-n) show a similar transport pattern for CO, suggesting that both SO<sub>2</sub> and CO within this plume were likely from anthropogenic sources in the same region. Forward trajectories tagged with OMI TRM SO<sub>2</sub> initiated at different levels (section 2.2) indicate that the plume height on 8 October was around 3 km. As shown in Figure 1 (f-i), the transport process could be roughly reproduced by the trajectory tracer model assuming SO<sub>2</sub> evenly distributed at 2.5-3.5 km AGL, although discrepancies exist between the model and satellite. The inconsistency is probably caused by uncertainties in both the initial SO<sub>2</sub> vertical profile and trajectory calculation. The actual SO<sub>2</sub> profile could be far more complicated than assumed, while the errors of trajectories grow with time and distance traveled. Nonetheless, the CALIPSO satellite flying over the plume (~38-42°N, Figure 3a) on the 8<sup>th</sup> detected an elevated aerosol layer centered at ~3 km, in agreement with our estimated initial SO<sub>2</sub> plume height. If aerosols and SO<sub>2</sub> were from the same source region (a reasonable assumption for this season), or if the elevated aerosol layer was primarily comprised of sulfate formed during transport, one would expect the SO<sub>2</sub> and aerosols in the outflow plume to have similar altitude distributions. The pollution plume, as projected by the forward trajectories, would ascend to the 400-500 hPa pressure level (or ~5-6 km altitude) on 9 October, maintain at this height for another 24 hr, and then slowly descend to 500-

600 hPa before arriving at the west coast of North America. CALIPSO measurements were unavailable for these days.

To locate the source region of the plume, consider the weather pattern at 06 UTC on 6 October (Figure 4). A mid-latitude cyclone was found east of Lake Baikal, with a trough extending to its south-southeast and situated just west of the industrialized and densely populated northern China (35-40°N, 110-120°E). Pollutants often accumulate in the region under the relatively stagnant conditions ahead of cold fronts [e.g., *Li et al.*, 2007], and this case is no exception: satellite data show sizable SO<sub>2</sub> and CO (Figure 4) over the region on 6 October, despite both instruments' limited sensitivity to pollution in the lowest part of the atmosphere. The cyclone migrated eastward, with its cold front passing over northern China later on the 6<sup>th</sup>, while an upwind high pressure system started to settle into the area (see the sea level pressure at 18 UTC in Figure 5). Frontal lifting is expected as the cold front moved through northern China, but backward trajectories (Figure 5) did not show active upward motion until early on the 7<sup>th</sup> (-30 to -25 hr in trajectory time). The meteorological input to the trajectory model is probably too coarse to resolve the lifting early on the 6<sup>th</sup>. Nevertheless, as the aforementioned high pressure system moved into northern China early on the 7<sup>th</sup>, the trajectory air parcels were located to its southwest and traveled clockwise around it, before joining the strong southwesterly ascending flow associated with the cyclone between 12 and 18 UTC the same day (Figure S1). Some of the air parcels moved from below 900 hPa to 700 hPa in about 25-30 hr (Figure 5). If the subsequent ascent on 8-9 October is included, part of the plume was lifted from near the surface to 5-6 km, and traveled more than 15° longitude eastward and 15° latitude northward in 2-3 days. Such rapid ascent from the

lower atmosphere and northeastward movement are characteristics of warm conveyor belt (WCB), large-scale slantwise upward motion normally found along with mid-latitude cyclones [Eckhardt *et al.*, 2004]. WCB or frontal lifting thus appears to be the outflow mechanism for this case.

Once the plume is displaced from the source region into the free troposphere, the downstream meteorological pattern dictates, for the most part, its further transport. Figure 6 (top) clearly shows a cutoff low at the 500 hPa pressure level located just east of Japan on 9 October, which can also be identified at lower levels. The cutoff low persisted in the region for a few days, forcing the plume to first travel to the northeast. The most prominent feature over the East Pacific is a deep low over Alaska stretched well south of the Aleutian Islands. A strong Aleutian low with dense isobars and intense winds around it may facilitate transpacific transport [e.g., Liang *et al.*, 2005], as is the case with this particular plume (Figure 6, top).

In summary, the plume was lofted from its source region during late 6 October to early 7 October and arrived at North America on 11-12 October, spending a total of 5-6 days to cross the Pacific Ocean.

### 3.2 Cases 2 and 3

Similar analyses were also conducted for other two major transpacific events: case 2 in October 2008 (Figure 2b, from late 3 October to late 8 October, transit time: ~5 days) and case 3 in November 2010 (Figure 2c, from 6 November to 11-12 November, transit time: 5-6 days). Detailed description of the two cases is presented in the supplementary materials (Figures S2-S7). As with case 1, in both cases 2 and 3, plumes having enhanced SO<sub>2</sub> and CO were from northern China, and lifted into the FT by

WCB's associated with mid-latitude cyclones. The meteorological setup over the East Pacific (Figure 6, middle and bottom) featured a deep Aleutian low and a subtropical Pacific high to its south, favorable for the observed rapid transport.

### 3.3 Transpacific transit time and transport mechanism

In all three cases discussed above, the plumes spent 5-6 days to cross the Pacific, including 1-2 days for their ascent from the boundary layer into the FT. In comparison, *Jaffe et al.* [1999] reported transit time of ~6 days for transpacific transport observed over the Northwestern U.S. (tracer: CO, O<sub>3</sub>, PAN, radon, and non-methane hydrocarbons, NMHC). Likewise, aircraft measurements of CO and NMHC revealed transit time of 5-8 days for Asian plumes intercepted over the East Pacific [*de Gouw et al.*, 2004; *Barletta et al.*, 2009]. Similar transit time in spring was also derived from model simulations of transport at higher altitudes [e.g., *Holzer et al.*, 2003; *Yienger et al.* 2000]. Our reported transit time in autumn for the three episodes is largely comparable to the above studies on springtime events. Transpacific transit time as short as 2 days has been found for a few isolated summertime cases associated with deep convection [*Kritz et al.*, 1990; *Liang et al.*, 2007]. The former study used radon as a tracer while the latter observed a host of pollutants including CO, PAN, and NMHC.

The similarity in transit time between spring and autumn probably reflects the analogous transport mechanisms in the two seasons. Like many transpacific cases in spring, in all three autumn episodes studied here, mid-latitude cyclones and the associated warm conveyor belt were responsible for the Asian outflow. Pollution first built up near the surface under relatively stagnant conditions, and then was vented into the free troposphere by the upward movement induced by the approaching fronts. The mid-

latitude cyclones are generally more active in spring, but autumn as a transition season also sees frequent cyclonic activity. Once a plume is exported from its source region, the downstream meteorology regulates the destination and speed of the ensuing transport. Previous studies focusing on spring indicate that a deep Aleutian low and a north-south alignment between the Aleutian low and Pacific subtropical high would create a more zonal flow favoring rapid transport across the Pacific [e.g., *Liang et al.*, 2005], and our analysis for autumn reaches the same conclusion.

### 3.4 Transport efficiency of SO<sub>2</sub>

A major rainmaker, WCB may produce sizable amount of precipitation [e.g., *Eckhardt et al.*, 2004] and substantial washout of soluble species is expected during the ascent within WCB. Indeed, clouds were clearly visible near the fronts and the TRMM (Tropical Rainfall Measuring Mission) satellite detected rainfall at the initial stage of all three cases (on 8 October, 2006, 4 October, 2008, and 8 November, 2010). Under polluted prefrontal conditions, aircraft typically measured ~1-2 DU of SO<sub>2</sub> over northern China [e.g., *Dickerson et al.*, 2007; *He et al.*, 2011]. Given the low SO<sub>x</sub> export efficiency (15-20%) previously estimated for Asian FT outflow [*Koike et al.*, 2003], the SO<sub>2</sub> loading (~0.5 DU) observed by OMI over the remote Pacific (Figures 1, S2, and S5) in this study is truly remarkable. Assuming that all SO<sub>2</sub> was within a ~1.5 km thick layer at around 500 hPa, this would translate into a mixing ratio of several ppb. Even if overestimated by a factor of two by the operational retrieval algorithm, the SO<sub>2</sub> loading of the plumes is still substantial. Note that to quantify the transport efficiency of SO<sub>2</sub> using satellite data, one has to take into account several factors, particularly the change of SO<sub>2</sub> signal during

transport, the detection limit of the satellite sensor, and the interference of aerosols and clouds, as detailed in our previous case study [Li *et al.*, 2010b].,

As mentioned in section 1, there is observational evidence that part of the SO<sub>2</sub> can escape scavenging during wet lifting and travel over long distances. During TRACE-P, several plumes at 2-4 km with ~1 ppb of SO<sub>2</sub> were observed over the central North Pacific [Tu *et al.*, 2004]. Brock *et al.* [2004] measured up to 0.6 ppb of SO<sub>2</sub> and high concentrations of H<sub>2</sub>SO<sub>4</sub> near the California coast during the ITCT 2K2 campaign, after the plume had encountered significant cloud formation and precipitation. They proposed that prior to the ascent, a fraction of SO<sub>2</sub> reacted to form sulfate, which would be efficiently scavenged during the frontal lifting; because of its modest solubility, some of the unreacted SO<sub>2</sub> could survive the wet removal process, and generate H<sub>2</sub>SO<sub>4</sub> during the ensuing long-range transport in the FT. Note that the amount of transported SO<sub>2</sub> measured in the above aircraft experiments is much smaller than observed in our cases. Our study thus not only provides further evidence that anthropogenic SO<sub>2</sub> can travel far away from Asia, but also suggests that the magnitude of such transport can be far greater than implied by previous measurements.

We also examined the OMI-retrieved NO<sub>2</sub> column amounts in the three cases. Long-range transport of NO<sub>x</sub> has been observed from satellites [e.g., Stohl *et al.*, 2003], but little evidence was found here. The oxidation of NO<sub>x</sub> to HNO<sub>3</sub> and PAN is relatively fast. The highly soluble HNO<sub>3</sub> is expected to be washed out during the frontal lifting, while PAN has been identified as the dominant NO<sub>y</sub> species in the Asian outflow [e.g., Miyazaki *et al.*, 2003]. Overall, only 10-20% of Asian NO<sub>y</sub> is exported to the FT, with even less in the form of NO<sub>x</sub> [e.g., Koike *et al.*, 2003; Miyazaki *et al.*, 2003; Nowak *et al.*,

2004; Walker *et al.*, 2010]. Some highly reactive VOCs may similarly form organic aerosols that will be scavenged during the ascent [Brock *et al.*, 2004]. Because of the relative enrichment of SO<sub>2</sub> in the FT, sulfate and dust are often the dominant aerosol species in Asian plumes captured near North America [e.g., van Donkelaar *et al.*, 2008]. Our results for autumn are consistent with these springtime measurements, and imply that SO<sub>2</sub> emissions from East Asia probably have greater direct impact on the downstream aerosol loading than other combustion products.

#### 4. The frequency of SO<sub>2</sub> long-range transport events

##### 4.1 Determination of the frequency of SO<sub>2</sub> long-range transport in autumn using A-train data

Section 3 demonstrates the potential of combining satellite observations of CO and SO<sub>2</sub> in studying long-range transport of anthropogenic pollution. A relatively long-lived pollutant, CO is mainly released from incomplete fuel combustion, while the relatively short-lived SO<sub>2</sub> is primarily emitted from coal burning. Since SO<sub>2</sub> from biomass burning and CO from volcanic eruptions are relatively small, simultaneous observations of these two gases allow us to distinguish between industrial and biomass burning sources, and between anthropogenic and volcanic plumes. Significant anthropogenic SO<sub>2</sub> plumes over the remote Pacific Ocean are also strong evidence for rapid transport from Asia. Another advantage of using AIRS CO and OMI SO<sub>2</sub> data is that the coverage of the two retrievals is less influenced by cloudy scenes, although plumes underneath thick clouds will still be undetectable. Aerosol retrievals using MODIS sensors have proved valuable for studying long-range transport, but for all three

cases discussed above the availability of MODIS retrievals was severely limited over the North Pacific storm track.

We extended our analysis to SON (September, October, and November) of 2005-2008 to estimate the frequency of SO<sub>2</sub> long-range transport (LRT). Daily AIRS CO and OMI TRM SO<sub>2</sub> data gridded to 1° × 1° resolution were employed to search for outflow and LRT plumes. The Asian plumes discussed in section 3 were all first spotted over Northeast Asia (northeastern China, Russian Far East, and Japan), and the Asian outflow region (Figure 7a) was defined accordingly. Our predefined long-range transport (LRT) receptor region covered the domain of 25-60°N, 120-150°W (Figure 7e).

We first looked for outflow plumes with at least 10 grid cells in the outflow region having both enhanced CO ( $\geq 2.5 \times 10^{18}$  molecules/cm<sup>2</sup>) and SO<sub>2</sub> ( $\geq 0.2$  DU). Only a single plume was allowed per day and consecutive days with a plume identified were screened to minimize multiple counting. The criterion for CO is close to the season-mean AIRS CO column amount over northern China, the most important source region identified in section 3. As for SO<sub>2</sub>, it was assumed that the spatial averaging would reduce the 1- $\sigma$  noise from 0.3 DU (section 2) to ~0.05 DU, and the detection limit for SO<sub>2</sub> can be roughly estimated at 0.2 DU (signal-to-noise ratio S:N = 2:1 for  $\pm 1\sigma$  noise). A total of 62 outflow plumes satisfying the above criteria were found for our study period. This count is quite sensitive to the selected criterion for CO: increasing and decreasing it by 10% would change the total count to 39 and 113, respectively. Increasing (decreasing) the threshold for SO<sub>2</sub> by 10%, on the other hand, only decreases (increases) the number of counted outflow plumes to 60 (67).

The LRT events were defined as those days with at least 10 grid cells in the receptor region having  $\text{CO} \geq 2.25 \times 10^{18}$  molecules/cm<sup>2</sup> and  $\text{SO}_2 \geq 0.2$  DU. Since the CO column amounts became smaller as the plumes crossed the Pacific (section 3), we used a 10% lower criterion for CO for LRT plumes. Other criteria including that for  $\text{SO}_2$  remained identical to ensure that only plumes with strong  $\text{SO}_2$  signals were included. Additionally, the identified LRT plumes were checked to ensure that they were not originated from North America. We counted a total of 16 LRT events in autumn for the 4-year period. As with outflow plumes, the frequency of LRT plumes was found to be sensitive to the criterion for CO. 29 (13) plumes were found if it was adjusted down (up) by  $0.05 \times 10^{18}$  molecules/cm<sup>2</sup>. Increasing (decreasing) the threshold for  $\text{SO}_2$  by 10% changes the number of counted LRT plumes to 14 (18). Note that the number of outflow and LRT plumes is likely underestimated especially for November, due to the gap in data coverage at high latitudes (*cf.* Figure 7).

One can also estimate how often strong  $\text{SO}_2$  and CO signals are detected over a specific grid cell to determine the spatial distribution of outflow or LRT plumes. The results presented in Figure 7 indicate that the primary outflow pathway for Asian pollution in the season is the area around the Sea of Japan, where the outflow frequency is ~5% (Figure 7a). This means that about 5% of the time during the study period (or ~18 days), strong plumes with  $\text{SO}_2 \geq 0.2$  DU and  $\text{CO} \geq 2.5 \times 10^{18}$  molecules/cm<sup>2</sup> were captured over this area by satellite sensors. For the receptor region, the latitude band of 35-55°N appears to be the most important inflow area for LRT plumes. The frequency of strong pollution plumes ( $\text{SO}_2 \geq 0.2$  DU,  $\text{CO} \geq 2.25 \times 10^{18}$  molecules/cm<sup>2</sup>) in the area is mostly ~1-2%, but exceeds 3% for ~10% of the grid cells. In other words, for areas most

susceptible to the influence of LRT, Asian plumes were found on over 10 days during the study period.

Both outflow and LRT events also demonstrate substantial temporal variation, with more episodes observed in October and November than in September (Figure 7). More precipitation over the outflow region in September (Figure 8b) is probably an important reason for this temporal variation. Other factors such as the frequency of frontal lifting events and the atmospheric lifetime of SO<sub>2</sub> may also play a role. The mean AIRS CO loading over northern China is largely constant through the three months, and the OMI SO<sub>2</sub> over the outflow region is much smaller in September. The choice of CO criterion is therefore unlikely the predominant reason for our observed temporal variation.

#### 4.2 Comparison to the results using IASI and the seasonal change in transport frequency

More recently, *Clarisse et al.* [2011] utilized IASI, an infrared satellite sensor, to study the long-range SO<sub>2</sub> transport case in November 2010 (case 3 in our study), and came to the same conclusion as ours (from the hyperspectral UV OMI instrument) that WCB lifting was the responsible mechanism. Their inspection of the IASI retrievals during October 2007–December 2010 led to 12 LRT episodes in autumn, 10 in winter, and only 3 in spring. The count of 12 LRT plumes in almost 4 complete fall seasons is comparable to our results, as is their criterion for SO<sub>2</sub> loading (~0.186 DU). But they focused on plumes above 5 km in altitude, and defined those that can be tracked for  $\geq 2.5$  days as LRT cases. Considering the typical transpacific transit time of 5-6 days as discussed in section 3, some of their cases probably won't be classified as LRT events using our method. Both OMI and IASI have limited sensitivity to SO<sub>2</sub> at lower altitudes,

and would underestimate the frequency of the actual SO<sub>2</sub> LRT events. OMI is relatively more sensitive and can detect plumes well below 5 km (as shown in our case studies), and our count based on OMI data is probably a closer lower-limit for the frequency of LRT events.

Larger discrepancy exists between the two satellite data sets for the spring season. Contrary to the finding of *Clarisse et al.* [2011], our preliminary results (Figure S8) suggest that the outflow and long-range transport of SO<sub>2</sub> are probably more active in spring than in autumn. While the two seasons have similar number of the frontal lifting events [*Liang et al.*, 2004], autumn is slightly wetter over the major source and outflow regions (Figure S9). Therefore one would expect the SO<sub>2</sub> transport to be more active in spring. However, a large difference in the abundance of CO can be found between the two seasons, and the CO criteria used in our preliminary analysis for spring will need to be further refined (*cf.* supplementary materials) before a definite conclusion can be drawn. *Clarisse et al.* [2011] also hypothesized that the plume transport height in spring could be lower, causing a low bias in IASI-observed transport frequency. Another fundamental difference between the two seasons is the much larger dust loading in spring, which may influence the transport efficiency of SO<sub>2</sub>. If co-located, dust particles may provide the site for heterogeneous reactions of SO<sub>2</sub> [e.g. *Usher et al.*, 2002], and could possibly increase the solubility of SO<sub>2</sub> in cloud droplets by decreasing their acidity. Dust may also interfere with satellite retrievals, decreasing the sensitivity of satellite sensors to SO<sub>2</sub> [e.g., *Krotkov et al.*, 2008]. A comprehensive study comparing the two seasons would be necessary to fully understand the seasonal change in SO<sub>2</sub> long-range transport from Asia.

## 5. Conclusions

We investigated rapid transpacific transport in autumn using multiple sensors of the A-train satellite constellation. For typical cases discussed in section 3, pollution plumes with high concentrations of SO<sub>2</sub> were observed over the North Pacific Ocean by the OMI instrument, and found to travel from their source regions in East Asia to North America within 5-6 days. The AIRS instrument showed very similar transport patterns for CO, suggesting that these plumes were most likely derived from anthropogenic sources. Trajectory analysis along with meteorological data indicate that, similar to many springtime transpacific events, strong lifting in the warm conveyor belt of mid-latitude wave cyclones is the main outflow mechanism for these autumn events, while the strength and relative position of the Aleutian low and Pacific subtropical high largely determine the timescale and pathway for further transport. Dry (non-precipitating) convection induced by cold fronts could be another efficient export mechanism for Asian pollutants [Dickerson *et al.*, 2007], but is not explicitly resolved in the satellite data and trajectory model used in this study. The A-train observations provide evidence that in some cases much of the SO<sub>2</sub> could escape scavenging during the ascent in WCB, and be transported at greater efficiency than NO<sub>x</sub>. The spatial coverage and magnitude of these SO<sub>2</sub> transport events far exceed those previously recorded in the sparse springtime aircraft experiments, suggesting that Asian sulfur emissions may have large impacts over vast downstream regions.

An analysis utilizing the AIRS CO and OMI SO<sub>2</sub> data from September, October, and November of the 2005-2008 period reveals 16 SO<sub>2</sub> long-range transport events, out of 62 outflow episodes from East Asia. The most important Asian outflow pathway for

the season is the area around the Sea of Japan, while the long-range transport plumes most frequently influence the latitudes between 35°N and 55°N over the East Pacific. While the plume counts are sensitive to the choice of criteria, and satellite observations likely underestimate the frequency of transport events, our results undoubtedly point to the importance of long-range transport from Asia in autumn.

The approach employed in this study can be applied to other seasons. Our preliminary analysis suggests that the long-range transport of Asian anthropogenic SO<sub>2</sub> could be even more active in spring. Differences in frontal lifting, precipitation, and dust loading may result in the seasonal change in the SO<sub>2</sub> transport efficiency and frequency. For future studies, we plan to employ SO<sub>2</sub> data from a new retrieval algorithm [Yang *et al.*, 2010], whose improved accuracy has been demonstrated in recent airborne validation measurements over central China [He *et al.*, 2011]. In addition to the OMI SO<sub>2</sub> and AIRS CO data, we will make use of other satellite data such as the Aerosol Index [Hsu *et al.*, 1996] for detecting dust moving along with pollution. It will also be interesting to examine whether the satellite-observed long-range transport events can be reproduced by chemical transport models. Such intercomparison can help evaluate the model output, while the combination of the two may lead to more robust estimates on the frequency of transpacific SO<sub>x</sub> transport events, their controlling factors, and their impacts.

### **Acknowledgements**

The OMI and AIRS data used in this study were acquired as part of the activities of NASA's Science Mission Directorate, and are archived and distributed by the Goddard Earth Sciences (GES) Data and Information Services Center (DISC). CALIPSO data were acquired from the Atmospheric Science Data Center (ASDC) at NASA Langley

Research Center. The authors wish to thank Dr. Russell R. Dickerson of University of Maryland and the anonymous reviewers for helpful comments. This study was partially supported by the NASA Radiation Sciences Program managed by Dr. Hal Maring.6.

## References

- Aumann, H. H., et al., (2003), AIRS/AMSU/HSB on the aqua mission: Design, science objectives, data products, and processing systems, *IEEE Trans. Geosci. Remote Sens.*, 41(2), 253-264.
- Barletta, B., et al. (2009), Characterization of volatile organic compounds (VOCs) in Asian and north American pollution plumes during INTEX-B: identification of specific Chinese air mass tracers, *Atmos. Chem. Phys.*, 9, 5371–5388.
- Berntsen, T. K., S. Karlsdóttir, and D. A. Jaffe (1999), Influence of Asian emissions on the composition of air reaching the north western United States, *Geophys. Res. Lett.*, 26(14), 2171–2174, doi:10.1029/1999GL900477.
- Bey, I., D. J. Jacob, J. A. Logan, and R. M. Yantosca (2001), Asian chemical outflow to the Pacific in spring: Origins, pathways, and budgets, *J. Geophys. Res.*, 106, D19, 23097-23113.
- Bhartia, P. K. and C. W. Wellemeyer (2002), OMI TOMS-V8 Total O3 Algorithm, *Algorithm Theoretical Baseline Document: OMI Ozone Products*, edited by P. K. Bhartia, vol. II, ATBD-OMI-02, version 2.0.
- Brock, C. A., et al. (2004), Particle characteristics following cloud-modified transport from Asia to North America, *J. Geophys. Res.*, 109, D23S26, doi:10.1029/2003JD004198.

- Brown-Steiner, B. E. and P. G. Hess (2011), Asian influence on surface ozone in the United States: a comparison of chemistry, seasonality, and transport mechanisms, *J. Geophys. Res.*, doi:10.1029/2011JD015846, in press.
- Carmichael, G. R., et al. (2003), Evaluating regional emission estimates using the TRACE-P observations, *J. Geophys. Res.*, 108(D21), 8810, doi:10.1029/2002JD003116.
- Chin, M., T. Diehl, P. Ginoux, and W. Malm (2007), Intercontinental transport of pollution and dust aerosols: implications for regional air quality, *Atmos. Chem. Phys.*, 7, 5501–5517.
- Clarisse, L., M. Fromm, Y. Ngadi, L. Emmons, C. Clerbaux, D. Hurtmans, and P. F. Coheur (2011), Intercontinental transport of anthropogenic sulfur dioxide and other pollutants: An infrared remote sensing case study, *Geophys. Res. Lett.*, 38, L19806, doi:10.1029/2011GL048976.
- Cooper, O. R., et al. (2004), A case study of transpacific warm conveyor belt transport: Influence of merging airstreams on trace gas import to North America, *J. Geophys. Res.*, 109, D23S08, doi:10.1029/2003JD003624.
- Cooper, O. R., et al. (2010), Increasing springtime ozone mixing ratios in the free troposphere over western North America, *Nature*, 463, 344-348, doi:10.1038/nature08708.
- de Gouw, J. A., et al. (2004), Chemical composition of air masses transported from Asia to the U.S. West Coast during ITCT 2K2: Fossil fuel combustion versus biomass-burning signatures, *J. Geophys. Res.*, 109, D23S20, doi:10.1029/2003JD004202.

- Di Pierro, M., L. Jaeglé, and T. L. Anderson (2011), Satellite observations of aerosol transport from East Asia to the Arctic: three case studies, *Atmos. Chem. Phys.*, 11, 2225–2243.
- Dickerson, R. R., et al. (2007), Aircraft observations of dust and pollutants over northeast China: Insight into the meteorological mechanisms of transport, *J. Geophys. Res.*, 112, D24S90, doi:10.1029/2007JD008999.
- Draxler, R. R., and G. D. Rolph (2003), HYSPLIT (HYbrid Single-Particle Lagrangian Integrated Trajectory) Model, NOAA ARL READY Web site <http://www.arl.noaa.gov/ready/hysplit4.html>.
- Dunlea, E. J., et al. (2009), Evolution of Asian aerosols during transpacific transport in INTEX-B, *Atmos. Chem. Phys.*, 9, 7257–7287.
- Eckhardt, S., A. Stohl, H. Wernli, P. James, C. Forster, and N. Spichtinger (2004), A 15-year climatology of warm conveyor belts, *J. Climate*, 17, 218–236.
- Fiore, A. M., et al. (2009), Multimodel estimates of intercontinental source-receptor relationships for ozone pollution, *J. Geophys. Res.*, 114, D04301, doi:10.1029/2008JD010816.
- Fisher, J. A., et al. (2010), Source attribution and interannual variability of Arctic pollution in spring constrained by aircraft (ARCTAS, ARCPAC) and satellite (AIRS) observations of carbon monoxide, *Atmos. Chem. Phys.*, 10, 3479–3494.
- He, H., et al. (2011), Measurements and numerical simulations of tropospheric SO<sub>2</sub> and sulfate aerosols: A case study of sulfur compounds over central China, *J. Geophys. Res.*, revised.

- Heald, C. L., D. J. Jacob, R. J. Park, B. Alexander, T. D. Fairlie, R. M. Yantosca, and D. A. Chu (2006), Transpacific transport of Asian anthropogenic aerosols and its impact on surface air quality in the United States, *J. Geophys. Res.*, 111, D14310, doi:10.1029/2005JD006847.
- Holzer, M., I. G. McKendry, and D. A. Jaffe (2003), Springtime trans-Pacific atmospheric transport from east Asia: A transit-time probability density function approach, *J. Geophys. Res.*, 108(D22), 4708, doi:10.1029/2003JD003558.
- Hsu, N. C., J. R. Herman, P. K. Bhartia, C. J. Seftor, O. Torres, A. M. Thompson, J. F. Gleason, T. F. Eck, and B. N. Holben (1996), Detection of biomass burning smoke from TOMS measurements, *Geophys. Res. Lett.*, 23(7), 745–748.
- Huffman, G. J., R. F. Adler, M. M. Morrissey, D. T. Bolvin, S. Curtis, R. Joyce, B. McGavock, and J. Susskind (2001), Global precipitation at one-degree daily resolution from multisatellite observations, *J. Hydrometeor.*, 2(1), 36-50.
- Jacob, D. J., J. A. Logan, and P. P. Murti (1999), Effects of rising Asian emissions on surface ozone in the United States, *Geophys. Res. Lett.*, 26 (14), 2175-2178.
- Jacob, D. J., J. H. Crawford, M. M. Kleb, V. S. Connors, R. J. Bendura, J. L. Raper, G. W. Sachse, J. C. Gille, L. Emmons, and C. L. Heald (2003), Transport and Chemical Evolution over the Pacific (TRACE-P) aircraft mission: Design, execution, and first results, *J. Geophys. Res.*, 108(D20), 9000, doi:10.1029/2002JD003276.
- Jaffe, D., et al. (1999), Transport of Asian air pollution to North America, *Geophys. Res. Lett.*, 26(6), 711–714, doi:10.1029/1999GL900100.
- Jaffe, D., I. McKendry, T. Anderson, H. Price (2003), Six ‘new’ episodes of trans-Pacific transport of air pollutants, *Atmos. Environ.*, 37, 391–404.

- Joiner, J., and A. P. Vasilkov (2006), First results from the OMI Rotational Raman Scattering Cloud Pressure Algorithm, *IEEE Trans. Geosci. Rem. Sens.*, 44, 1272-1282.
- Kaneyasu, N., K. Takeuchi, M. Hayashi, S. Fujita, I. Uno, and H. Sasaki (2000), Outflow patterns of pollutants from East Asia to the North Pacific in the winter monsoon, *J. Geophys. Res.*, 105(D13), 17361–17377, doi:10.1029/2000JD900138.
- Koike, M., et al. (2003), Export of anthropogenic reactive nitrogen and sulfur compounds from the East Asia region in spring, *J. Geophys. Res.*, 108(D20), 8789, doi:10.1029/2002JD003284.
- Kritz, M. A., J.-C. Le Roulley, and E. F. Danielsen (1990), The China clipper – fast advective transport of radon-rich air from the Asian boundary layer to the upper troposphere near California, *Tellus*, 42B, 46-61.
- Krotkov, N.A., S.A. Carn, A.J. Krueger, P.K. Bhartia, and K. Yang (2006), Band residual difference algorithm for retrieval of SO<sub>2</sub> from the Aura Ozone Monitoring Instrument (OMI). *IEEE Trans. Geosci. Remote Sensing*, 44(5), 1259-1266, doi:10.1109/TGRS.2005.861932.
- Krotkov, N. A., et al. (2008), Validation of SO<sub>2</sub> retrievals from the Ozone Monitoring Instrument over NE China, *J. Geophys. Res.*, 113, D16S40, doi:10.1029/2007JD008818.
- Leaitch, W. R., et al. (2009), Evidence for Asian dust effects from aerosol plume measurements during INTEX-B 2006 near Whistler, BC, *Atmos. Chem. Phys.*, 9, 3523–3546.

- Levelt, P. F., G. H. J. van den Oord, M. R. Dobber, A. Mälkki, H. Visser, J. de Vries, P. Stammes, J. O. V. Lundell, and H. Saari (2006), The Ozone Monitoring Instrument, *IEEE Trans. Geosci. Rem. Sens.*, 44, 1093-1101.
- Li, C., L. T. Marufu, R. R. Dickerson, Z. Li, T. Wen, Y. Wang, P. Wang, H. Chen, and J. W. Stehr (2007), In situ measurements of trace gases and aerosol optical properties at a rural site in northern China during East Asian Study of Tropospheric Aerosols: An International Regional Experiment 2005, *J. Geophys. Res.*, 112, D22S04, doi:10.1029/2006JD007592.
- Li, C., Q. Zhang, N. A. Krotkov, D. G. Streets, K. He, S.-C. Tsay, and J. F. Gleason (2010a), Recent large reduction in sulfur dioxide emissions from Chinese power plants observed by the Ozone Monitoring Instrument, *Geophys. Res. Lett.*, 37, L08807, doi:10.1029/2010GL042594.
- Li, C., N. A. Krotkov, R. R. Dickerson, Z. Li, K. Yang, and M. Chin (2010b), Transport and evolution of a pollution plume from northern China: A satellite-based case study, *J. Geophys. Res.*, 115, D00K03, doi:10.1029/2009JD012245.
- Liang, Q., L. Jaeglé, D. A. Jaffe, P. Weiss-Penzias, A. Heckman, and J. A. Snow (2004), Long-range transport of Asian pollution to the northeast Pacific: Seasonal variations and transport pathways of carbon monoxide, *J. Geophys. Res.*, 109, D23S07, doi:10.1029/2003JD004402.
- Liang, Q., L. Jaeglé, and J. M. Wallace (2005), Meteorological indices for Asian outflow and transpacific transport on daily to interannual timescales, *J. Geophys. Res.*, 110, D18308, doi:10.1029/2005JD005788.
- Liang, Q., et al. (2007), Summertime influence of Asian pollution in the free troposphere

- over North America, *J. Geophys. Res.*, 112, D12S11, doi:10.1029/2006JD007919.
- Liu, H., D. J. Jacob, I. Bey, R. M. Yantosca, B. N. Duncan, and G. W. Sachse (2003), Transport pathways for Asian pollution outflow over the Pacific: Interannual and seasonal variations, *J. Geophys. Res.*, 108(D20), 8786, doi:10.1029/2002JD003102.
- Liu, Z., M. Vaughan, D. Winker, C. Kittaka, B. Getzewich, R. Kuehn, A. Omar, K. Powell, C. Trepte, and C. Hostetler (2009), The CALIPSO lidar cloud and aerosol discrimination: Version 2 algorithm and initial assessment of performance, *J. Atmos. Ocean. Technol.*, 26, 1198-1213.
- McMillan, W. W., K. Evans, C. Barnet, E. Maddy, G. Sachse, and G. Diskin (2011), Validating the AIRS Version 5 CO Retrieval With DACOM In Situ Measurements During INTEX-A and -B, *IEEE Trans. Geosci. Remote Sensing*, doi: 10.1109/TGRS.2011.2106505, in press.
- Miyazaki, Y., et al. (2003), Synoptic-scale transport of reactive nitrogen over the western Pacific in spring, *J. Geophys. Res.*, 108(D20), 8788, doi:10.1029/2002JD003248.
- Nowak, J. B., et al. (2004), Gas-phase chemical characteristics of Asian emission plumes observed during ITCT 2K2 over the eastern North Pacific Ocean, *J. Geophys. Res.*, 109, D23S19, doi:10.1029/2003JD004488.
- Park, R. J., D. J. Jacob, B. D. Field, R. M. Yantosca, and M. Chin (2004), Natural and transboundary pollution influences on sulfate-nitrate-ammonium aerosols in the United States: Implications for policy, *J. Geophys. Res.*, 109, D15204, doi:10.1029/2003JD004473.

- Parrish, D. D., Y. Kondo, O. R. Cooper, C. A. Brock, D. A. Jaffe, M. Trainer, T. Ogawa, G. Hübler, and F. C. Fehsenfeld (2004), Intercontinental Transport and Chemical Transformation 2002 (ITCT 2K2) and Pacific Exploration of Asian Continental Emission (PEACE) experiments: An overview of the 2002 winter and spring intensives, *J. Geophys. Res.*, 109, D23S01, doi:10.1029/2004JD004980.
- Pfister, G. G., L. K. Emmons, D. P. Edwards, A. Arellano, G. Sachse, and T. Campos (2010), Variability of springtime transpacific pollution transport during 2000–2006: the INTEX-B mission in the context of previous years, *Atmos. Chem. Phys.*, 10, 1345–1359.
- Rienecker, M. M., et al. (2011), MERRA - NASA's Modern-Era Retrospective Analysis for Research and Applications, *J. Climate*, 24, 3624–3648, doi: 10.1175/JCLI-D-11-00015.1.
- Rogers, R. R., et al. (2011), Assessment of the CALIPSO Lidar 532nm attenuated backscatter calibration using the NASA LaRC airborne High Spectral Resolution Lidar, *Atmos. Chem. Phys.*, 11, 1295–1311.
- Singh, H. B., W. H. Brune, J. H. Crawford, F. Flocke, and D. J. Jacob (2009), Chemistry and transport of pollution over the Gulf of Mexico and the Pacific: spring 2006 INTEX-B campaign overview and first results, *Atmos. Chem. Phys.*, 9, 2301-2318.
- Schoeberl, M. R., et al. (2006), Overview of the EOS Aura Mission, *IEEE Trans. Geosci. Rem. Sens.*, 44(5), 1066-1074, doi:10.1109/TGRS.2005.861950.
- Stohl, A., et al. (2003), Rapid intercontinental air pollution transport associated with a meteorological bomb, *Atmos. Chem. Phys.*, 3, 969–985.

- Tu, F. H., D. C. Thornton, A. R. Bandy, G. R. Carmichael, Y. Tang, K. L. Thornhill, G. W. Sachse, and D. R. Blake (2004), Long-range transport of sulfur dioxide in the central Pacific, *J. Geophys. Res.*, 109, D15S08, doi:10.1029/2003JD004309.
- Usher, C. R., H. Al-Hosney, S. Carlos-Cuellar, and V. H. Grassian (2002), A laboratory study of the heterogeneous uptake and oxidation of sulfur dioxide on mineral dust particles, *J. Geophys. Res.*, 107(D23), 4713, doi:10.1029/2002JD002051.
- van Donkelaar, A., et al. (2008), Analysis of aircraft and satellite measurements from the Intercontinental Chemical Transport Experiment (INTEX-B) to quantify long-range transport of East Asian sulfur to Canada, *Atmos. Chem. Phys.*, 8, 2999–3014.
- Walker, T. W., et al. (2010), Trans-Pacific transport of reactive nitrogen and ozone to Canada during spring, *Atmos. Chem. Phys.*, 10, 8353–8372.
- Winker, D. M., M. A. Vaughan, A. Omar, Y. Hu, K. A. Powell, Z. Liu, W. H. Hunt, and S. A. Young (2009), Overview of the CALIPSO mission and CALIOP data process algorithms, *J. Atmos. Ocean. Technol.*, 26, 2310-2323.
- Wuebbles, D. J., H. Lei, and J. Lin (2007), Intercontinental transport of aerosols and photochemical oxidants from Asia and its consequences, *Environ. Pollution*, 150, 65-84.
- Yang, K., N. Krotkov, A. Krueger, S. Carn, P. K. Bhartia, and P. Levelt (2007), Retrieval of large volcanic SO<sub>2</sub> columns from the Aura Ozone Monitoring Instrument (OMI): Comparisons and limitations, *J. Geophys. Res.*, 112, D24S43, doi:10.1029/2007JD008825.

- Yang, K., X. Liu, P. K. Bhartia, N. A. Krotkov, S. A. Carn, E. J. Hughes, A. J. Krueger, R. J. D. Spurr, and S. G. Trahan (2010), Direct retrieval of sulfur dioxide amount and altitude from spaceborne hyperspectral UV measurements: Theory and application, *J. Geophys. Res.*, 115, D00L09, doi:10.1029/2010JD013982.
- Yienger, J., M. Galanter, T. Holloway, M. Phadnis, S. Guttikunda, G. Carmichael, W. Moxim, and H. Levy II (2000), The episodic nature of air pollution transport from Asia to North America, *J. Geophys. Res.*, 105(D22), 26931-26945.
- Yu, H., L. A. Remer, M. Chin, H. Bian, R. G. Kleidman, and T. Diehl (2008), A satellite-based assessment of transpacific transport of pollution aerosol, *J. Geophys. Res.*, 113, D14S12, doi:10.1029/2007JD009349.
- Yurganov, L., W. McMillan, E. Grechko, and A. Dzhola (2010), Analysis of global and regional CO burdens measured from space between 2000 and 2009 and validated by ground-based solar tracking spectrometers, *Atmos. Chem. Phys.*, 10, 3479–3494.
- Zhang, L., et al. (2008), Transpacific transport of ozone pollution and the effect of recent Asian emission increases on air quality in North America: an integrated analysis using satellite, aircraft, ozonesonde, and surface observations, *Atmos. Chem. Phys.*, 8, 6117–6136.

**Figure Captions:**

**Figure 1.** Upper: OMI TRM SO<sub>2</sub> column amount (unit: DU) over Northeast Asia and the North Pacific at (a) 05 UTC on 8 October, (b) 03 UTC on 9 October, (c) 02 UTC on 10 October, (d) 00 UTC on 11 October, and (e) 23 UTC on 11 October 2006. Middle: tracer SO<sub>2</sub> (unit: DU) distribution calculated for the OMI observation time in (b-e), using

forward trajectories initiated on 8 October, and assuming SO<sub>2</sub> evenly distributed at 2.5-3.5 km (*cf.* section 2.2). Lower: AIRS CO column amount (unit: 10<sup>18</sup> molecules/cm<sup>2</sup>) observed almost simultaneously with OMI SO<sub>2</sub>. The blue lines in (a) and (j) mark the track of the CALIPSO satellite on 8 October.

**Figure 2.** The movement of the SO<sub>2</sub> plumes in (a) case 1: October 2006, (b) case 2: October 2008, and (c) case 3: November 2010 as observed by the OMI instrument. Colors represent the location of the plume center on different days, which is defined as the part of the plume having OMI TRM SO<sub>2</sub> ≥ 0.5 DU for 10/08-09/2006, 10/05/2008, and 11/08/2010; TRM SO<sub>2</sub> ≥ 0.35 DU for 10/10/2006, 10/06-07/2008, and 11/09-10/2011; and TRM SO<sub>2</sub> ≥ 0.25 UD for 10/11/2006.

**Figure 3.** CALIPSO vertical feature mask on (a) 8 October, indicating an aerosol layer aloft at ~2-4 km near 38-42 °N along the track in Figure 1a; (b) 6 October 2008, showing an aerosol layer at ~5 km near 45-47°N along the track in Figure S2b; (c) 9 November 2010, revealing an aerosol layer centered at ~3-6 km near 43-47°N along the track in Figure S5b; and (d) 10 November 2010, showing an aerosol layer at ~3-4 km near 42-44°N along the track in Figure S5c.

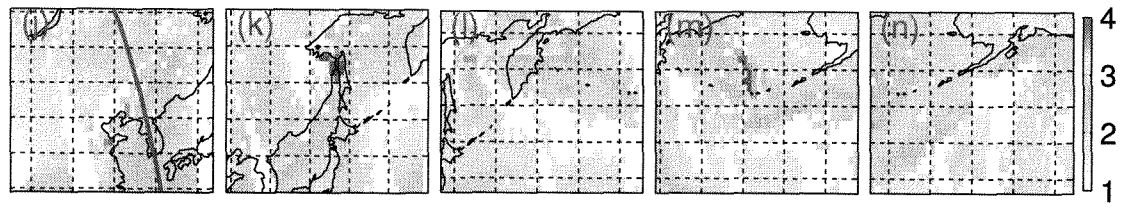
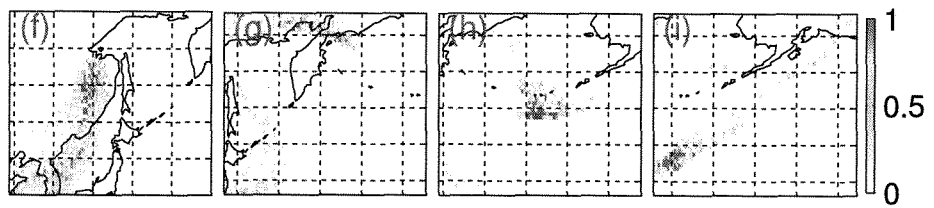
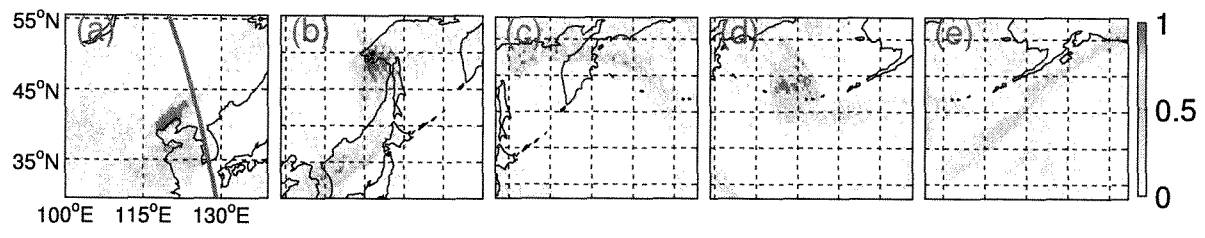
**Figure 4.** Left: OMI TRM SO<sub>2</sub> (color, unit: DU) at 05 UTC on 6 October 2006 and the MERRA 850 hPa geopotential height (blue lines) at 06 UTC. Right: AIRS CO column amount (color, unit: 10<sup>18</sup> molecules/cm<sup>2</sup>) and the MERRA 850 hPa wind vector (arrows) at approximately the same moment. Pollutants accumulated over northern China as a mid-latitude wave cyclone approached the region.

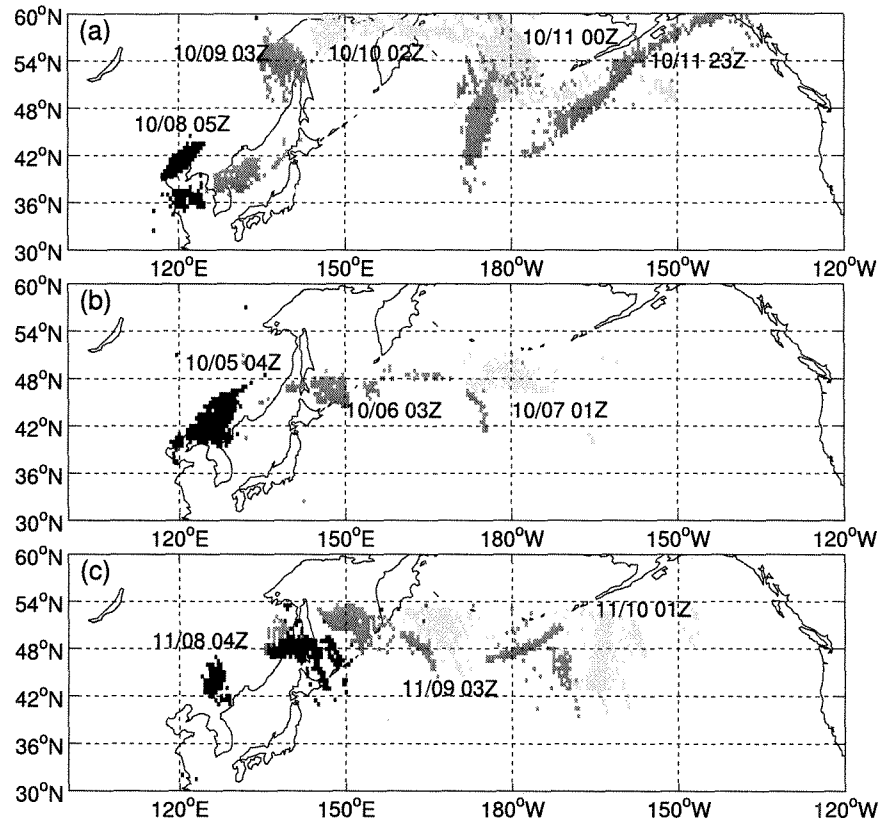
**Figure 5.** Upper: 36-hr backward trajectories calculated for grid cells with OMI TRM  $\text{SO}_2 \geq 1$  DU (stars). Trajectories are started at 05 UTC on 8 October 2006 from 3 km above ground level ( $\sim 700$  hPa). Dashed lines are the sea level pressure at 18 UTC on 6 October 2006 from the MERRA meteorological data. Lower: the height of trajectories indicates substantial ascent from the industrialized region in northern China induced by the cyclone.

**Figure 6.** MERRA 500 hPa geopotential height (contours) and wind field (vectors) at 00 UTC on (top) 9 October 2006, (middle) 6 October 2008, and (bottom) 9 November 2010.

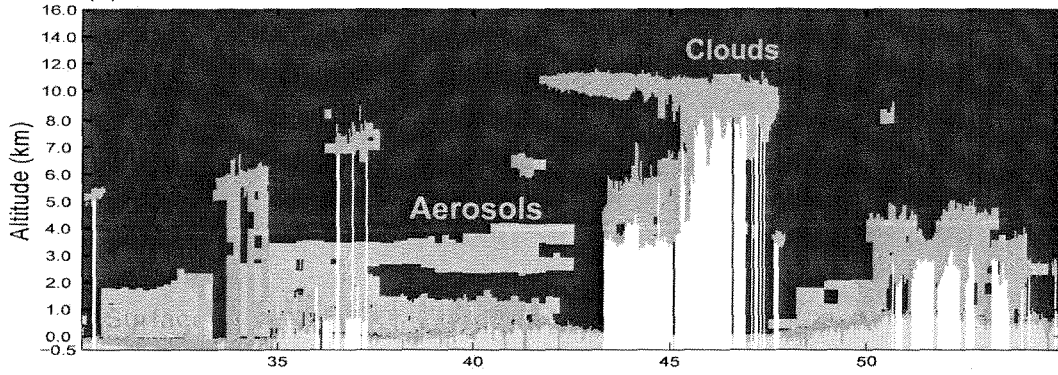
**Figure 7.** Upper row: the frequency of pollution plumes having OMI TRM  $\text{SO}_2 \geq 0.2$  DU and AIRS  $\text{CO} \geq 2.5 \times 10^{18}$  molecules/cm<sup>2</sup> for  $1^\circ \times 1^\circ$  grid cells over the Asian outflow region in (a) autumn, (b) September, (c) October, and (d) November during 2005-2008. Lower row: the frequency of pollution plumes having OMI TRM  $\text{SO}_2 \geq 0.2$  DU and AIRS  $\text{CO} \geq 2.25 \times 10^{18}$  molecules/cm<sup>2</sup> for  $1^\circ \times 1^\circ$  grid cells over the East Pacific long-range transport receptor region in (e) autumn, (f) September, (g) October, and (h) November during 2005-2008. The outflow and receptor regions are represented by the red boxes in the upper and lower rows, respectively. Gap in high latitudes in November is due to the elimination of OMI data with  $\text{SZA} > 70^\circ$  (*cf.*, section 2.1.1).

**Figure 8.** Mean precipitation (mm/day) from the Global Precipitation Climatology Project daily one-degree resolution data set [Huffman *et al.*, 2001] in (a) autumn, (b) September, (c) October, and (d) November during 2005-2008.

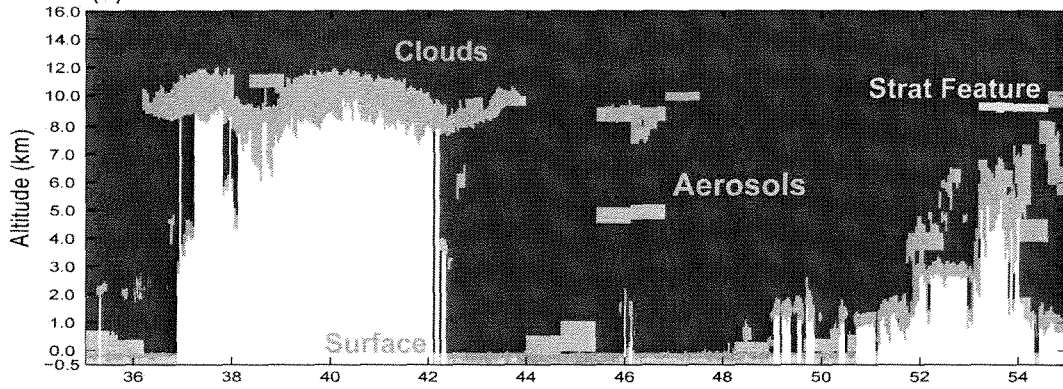




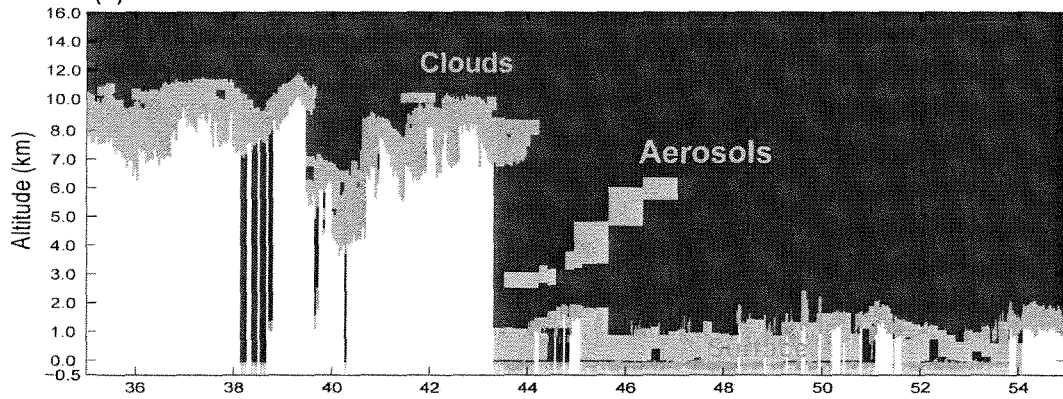
(a) October 2006



(b) October 2008



(c) November 2010



(d) November 2010

